Chaotic Radial Oscillations of a Harmonically Forced Gas Bubble, Parametric Dependence and Consequences for Sonoluminescence

Gábor Simon

February 2, 2000

NBI, Blegdamsvej 17 DK 2100, Copenhagen Ø, Denmark

Abstract

This study investigates the dynamics of a driven air bubble in water. It shows that depending on external parameters the radial oscillations of the bubble can be either stable or chaotic. The key to chaotic behaviour is identified to be due to nonzero amplitude of afterbounces at the beginning of the next acoustic cycle. In chaotic regime periodic orbit theory is successfully applied to calculate averages of relevant physical quantities, such as the air concentration at which the bubble is in diffusive equilibrium with the surrounding liquid. Finally the relevance to single bubble sonoluminescence is discussed.

1 Introduction

A gas bubble levitated in a liquid by ultrasound is an example of a highly nonlinear system, whose dynamics was known to be chaotic years before the first successful experiments could be realised. The theoretical study of the system goes back to Rayleigh who investigated the radial collapse of a spherical cavity in liquid [1] to explain the accelerated erosion of submarine fans during the I. World War. In the 80-ies the improvement of computer technology allowed to solve numerically the nonlinear equations describing the oscillations of harmonically forced gas bubbles, and the system was found to exhibit rich dynamics, such as period doubling bifurcations and chaos [4]. The study of the field was warped in 1990, after the discovery of single bubble sonoluminescence (SBSL) by Felipe Gaitan, who for the first time was able to levitate an air bubble in water and observed that it gave out flashes of light in every period of the oscillation. In contrast to earlier numerical studies the first experiments indicated a highly stable bubble dynamics, a synchronicity with the driving soundfield (typically ≈ 27 kHz) on the order of 50 ps. Later a few studies also reported period doubling, quasi-periodicity and chaos in the time series of successive flashes [5], [6], but the underlying mechanism was not yet been identified.

The aim of this term-paper is to study in depth the chaotic behaviour of the RP equation at chosen parameter values, to investigate the crossover from stable dynamics to chaos, and to give the parameter region of stability and its dependence on experimental conditions. Finally hopefully answer the question if radial bubble-dynamics is alone sufficient to explain the observed chaoticity.

2 The Rayleigh-Plesset Equation

The equation of motion for the interface-radius $R(t)$ of a spherically oscillating gas bubble under harmonical excitation is given by the Rayleigh-Plesset (RP) equation (for derivation see [1]). Its most frequently used form is

$$\begin{aligned}\rho_w(R\ddot{R}+\frac{3}{2}\dot{R}^2) &= P_g(R(t))-P_f(t)-P_0 \\ &+ \frac{R}{c_w}\frac{d}{dt}[P_g(R(t))-P_f(t)]-4\eta\frac{\dot{R}}{R}-\frac{2\sigma}{R},\end{aligned} \tag{1}$$

where the left-hand side is the inertial term, and the terms on the right-hand side give the various pressures acting on the interface. In particular $P_0 = 1bar$ is the static ambient pressure, $P_f = -P_a\sin(\omega t)$ is the forcing pressure with angular frequency ω and acoustic pressure amplitude P_a, and P_g is the uniform gas pressure inside the bubble, given by a van der Waals equation of state,

$$P_g(R(t)) = (P_0+\frac{2\sigma}{R_0})\frac{(R_0^3-a^3)^\gamma}{(R(t)^3-a^3)^\gamma}. \tag{2}$$

where R_0 is the ambient radius (stationary radius under normal temperature and pressure), $a = R_0/8.5$ is the hard core van der Waals radius for air, and γ is the polytropic exponent, which is 1 for an isothermic process, and greater than 1 for an adiabatic process, where the actual value depends on the choice of the gas. It must be noted that the assumption of uniformity is an approximation, but its validity is justified in most of the acoustic cycle. The material constants of water appearing in the RP equation are given in the following table*.

density	ρ_w	1000	kg/m^3
velocity of sound	c_w	1481	m/s
dynamic viscosity	η	1×10^{-3}	kg/ms
surface tension	σ	0.073	N/m

Table 1: Notation and room temperature-values of material constants in equation (1).

In order to solve numerically the RP-equation, it was transformed into the following set of first-order differential equations

$$\begin{aligned}\dot{R} &= V \\ \dot{V} &= \frac{1}{\rho_w R}(P_g-P_f-P_0-P_\eta-P_\sigma+P_s)-\frac{3}{2R}V^2,\end{aligned} \tag{3}$$

where the pressure terms defined as

$$P_f = -P_a\sin(\omega t) \qquad P_\eta = \frac{4\eta V}{R}, \qquad P_\sigma = \frac{2\sigma}{R}, \qquad P_s = \frac{R}{c_w}\frac{d}{dt}(P_g-P_f). \tag{4}$$

*When comparing with an experiment the value of 0.05 N/m is sometimes used for the surface tension, rather than the standard tabular value 0.073 N/m, thus taking into the account that in the experiments the water will always contain some amount of impurities, in which case it gives a better approximation.

As general remarks for the set of equations (3) it can be noted that they describe a highly nonlinear, non-autonomous dynamical system in a two-dimensional phase-space.

Since the explicit time dependence in (4) is harmonic, it is possible to transform the equations (3) into a coupled system of nonlinear and linear oscillators. Applying the same transformation as for the forced Brusselator in [9], the system will read

$$\begin{aligned}
\dot{R} &= V \\
\dot{V} &= \frac{1}{\rho_w R}(P_g + P_a Q - P_0 - P_\eta - P_\sigma + P_s) - \frac{3}{2R}V^2 \\
\dot{Q} &= \omega W \\
\dot{W} &= -\omega Q,
\end{aligned} \tag{5}$$

with fixed initial conditions $Q(t=0)=0$ and $W(t=0)=1$. The benefit of this form is that the dynamical system becomes autonomous, thus all the technics developed for such systems can be used. The price one have to pay is the increased dimension of the phase space.

The adjustable parameters, which were varied during the simulations are the amplitude of the forcing P_a, its angular frequency ω, and the ambient radius R_0. The numerical simulations them selves were carried out using a 5-th order Runge Kutta algorithm with adaptive stepsize-control applied, as described in [8]. If not otherwise mentioned, all the simulations used initial values of $R(t=0)=R_0$, $V(t=0)=0$, and the tabular values of the material constants..

3 Stability and Chaos

This section gives comparisons between stable and chaotic solutions to the RP equation and investigates some parametric dependence of the dynamics. Figure 1 shows a stable solution over one acoustic period, at parameter values ($P_a = 1.255 bar$, $R_0 = 5\mu m$, and $\omega/2\pi = 27kHz$) typical in SBSL experiments. The nonlinear oscillations of such bubbles are characterised by a big variety of spatial and temporal scales. Initially the radius is at its ambient value R_0. Then during the negative part of the sinusoidal driving the bubble slowly ($t_{exp} \approx 1/2T_p$) expands to its maximum ($\approx 10 \cdot R_0$). At this instant the pressure inside is almost vacuum. The increasing driving pressure then makes the bubble to collapse. The time to go from R_0 to the minimum radius is approximately given by the following formula [2]

$$t_c \approx \frac{\sqrt{6} R_0^{5/2}}{5 R_{max}^{3/2} (P_0/\rho_w)^{1/2}}. \tag{6}$$

For high forcing amplitudes the bubble at minimum reaches its hard core van der Waals radius ($R_0/8.5$), which results in enormous pressures and temperatures inside it (order of magnitudes: $10^4 bar$ and $10^4 K$) and also in a flash of light. In the late stages of the collapse the interface velocity can be even higher than the speed of the sound in the liquid which results in an outgoing shockwave in the water. The main collapse is followed by a sequence of afterbounces with decreasing amplitude, after which the whole process repeats itself precisely in the next acoustic cycle. The angular frequency of the afterbounces can

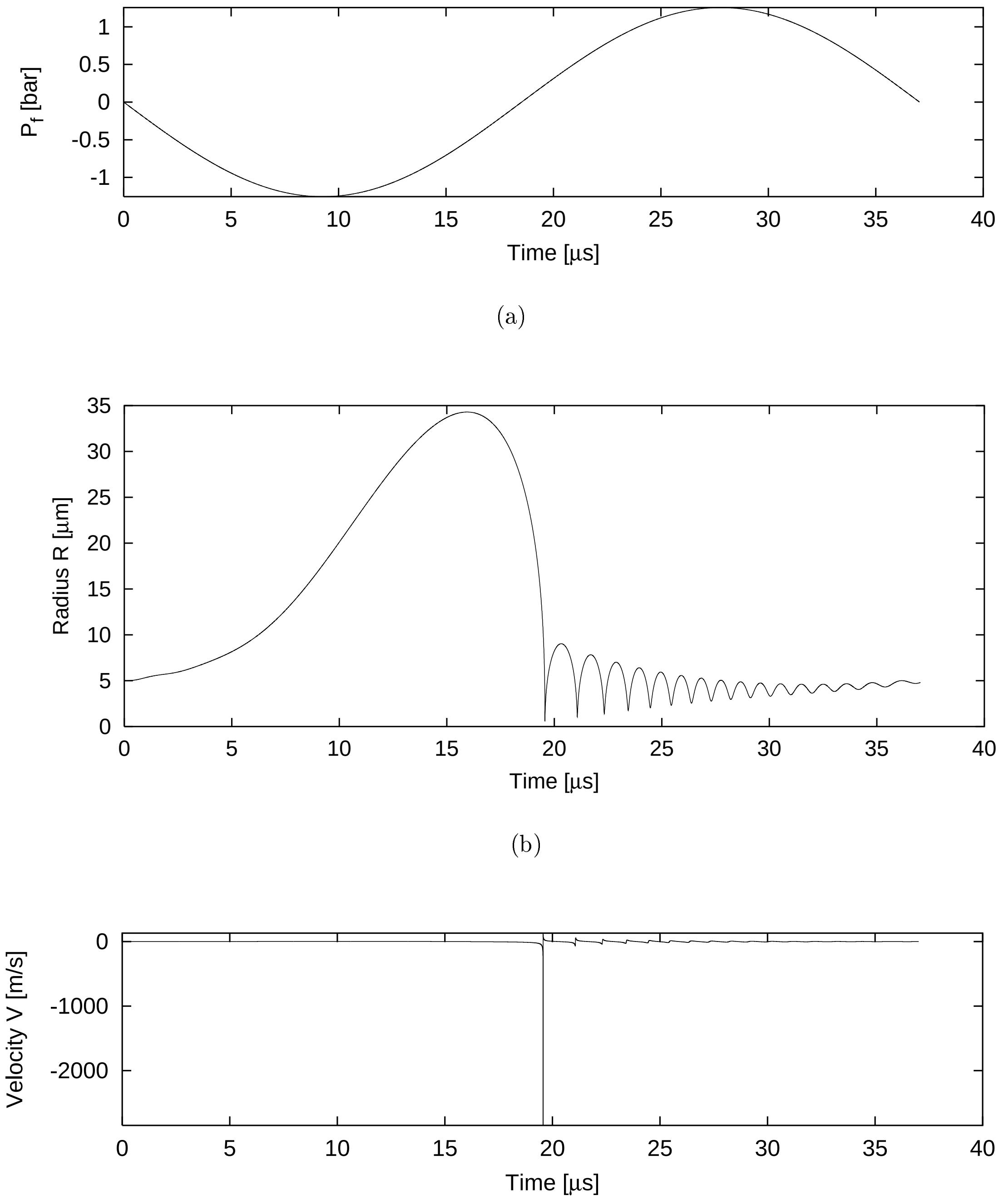

Figure 1: The driving pressure (a), the radius of the bubble (b), and the velocity of its interface (c) as a function of time for one acoustic cycle. The parameters are $P_a = 1.255 bar$, $R_0 = 5\mu m$, $\gamma = 1$, and $\omega/2\pi = 27kHz$.

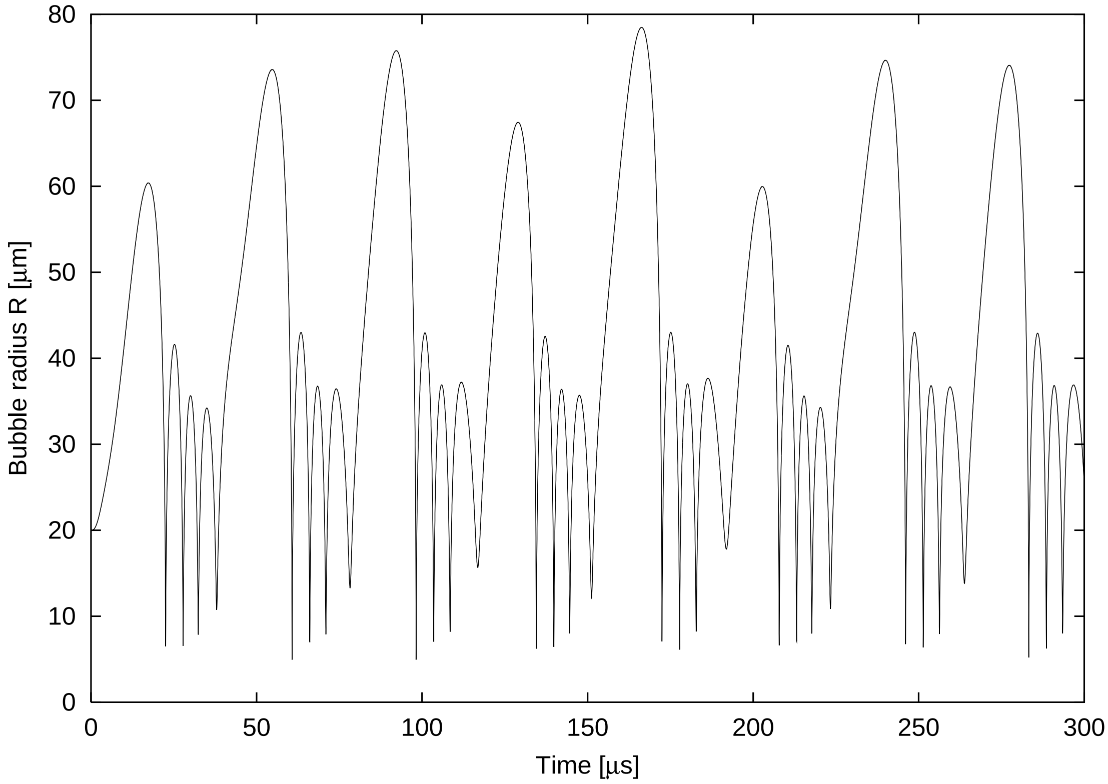

Figure 2: Radius of the bubble over 8 acoustic cycles. The parameters are $P_a = 1.255bar$, $R_0 = 20\mu m$, $\gamma = 5/3$, and $\omega/2\pi = 27kHz$.

be approximated with

$$\omega_b \approx \sqrt{\frac{1}{\rho_w R_0^2}(3\gamma(P_0 + \frac{2\sigma}{R_0}) - \frac{2\sigma}{R_0} - \frac{4\eta^2}{\rho_w R_0^2})}, \tag{7}$$

(see for instance [6]). An important feature of Fig. 1, which is also the reason of stability is that the amplitude of the afterbounces die away until the beginning of the next cycle and thus the radius at the end of the cycle has its initial value.

If the ambient radius is increased to $R_o = 20\mu m$ and the value of the polytropic exponent is changed to $\gamma = 5/3$, the solution to the RP equation shifts to the chaotic regime. Figure 2 shows the oscillations of the bubble over 8 acoustic periods. This regime differs from the stable solution in several aspects. Probably the most important is that due to the increased R_0 the angular frequency of the afterbounces decreased. As a result there is not enough time for the afterbounces to be damped out completely before the next expansion begins. Thus each new acoustic cycle will have the "memory" of the undamped amplitude from the previous cycle, which results in big variations in the maximum radiuses. In particular the $\omega_b \approx 3 \times \omega$ in Fig. 2 is in good agreement with equation (7). The attractor in the phase space (R, V) is shown in Fig. 3. A magnification of the attractor around the maximal radius shows that the trajectory fills up the phase space between $60\mu m$ and $80\mu m$.

After chaos is found at a particular point in the parameter space $(P_a, R_0, \omega/2\pi)$ it is interesting to investigate how the system behaves upon changing these parameters.

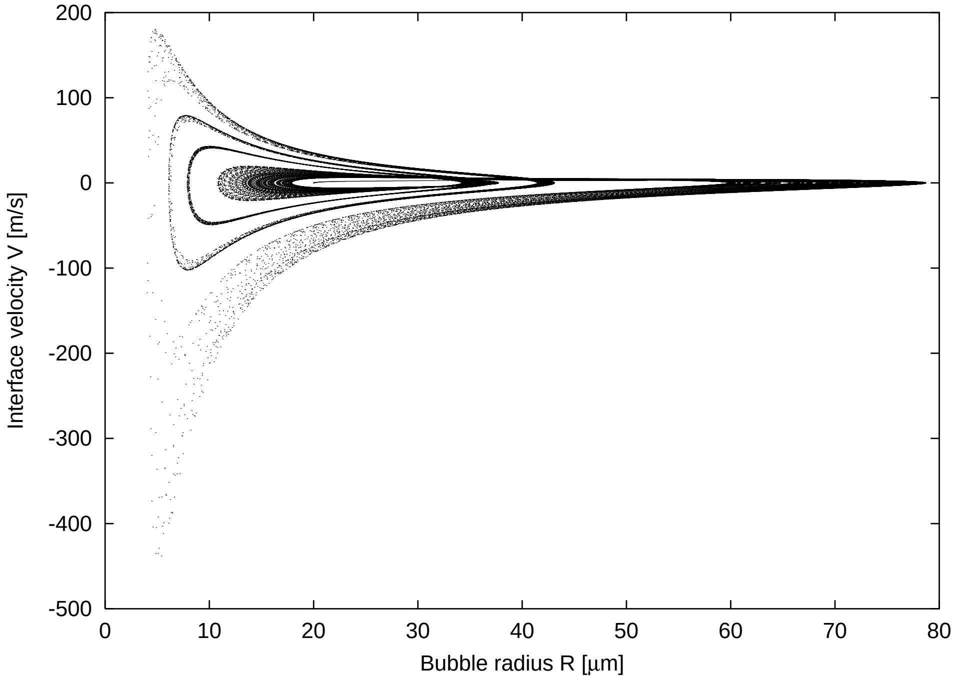

(a)

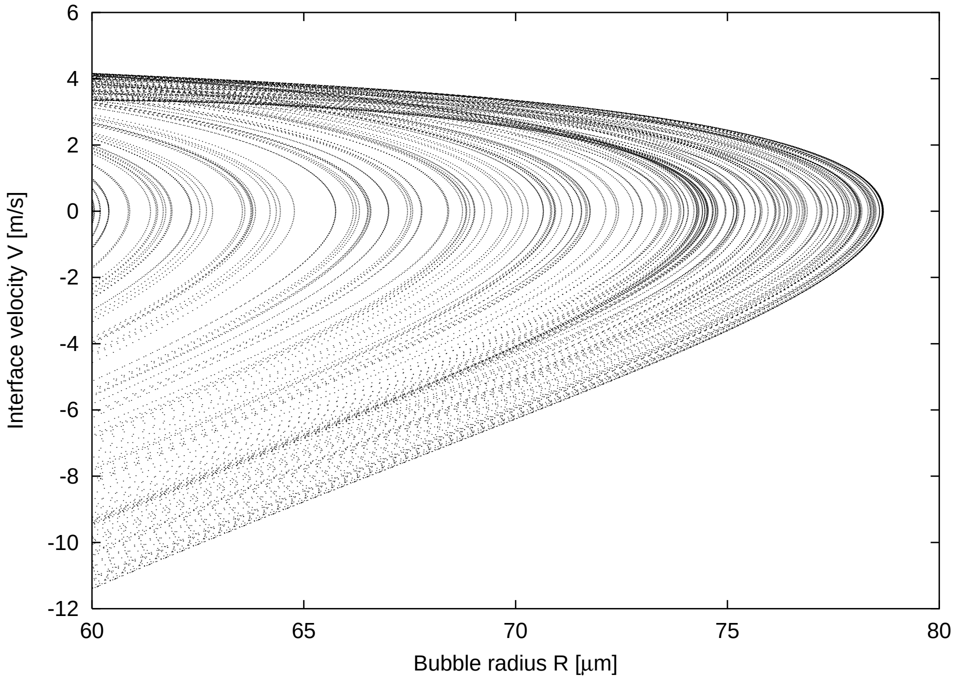

(b)

Figure 3: The chaotic attractor (a) and a region blown up around the maximal radius (b) for 100 cycles. The parameters are $P_a = 1.255 bar$, $R_0 = 20\mu m$, $\gamma = 5/3$, and $\omega/2\pi = 27kHz$.

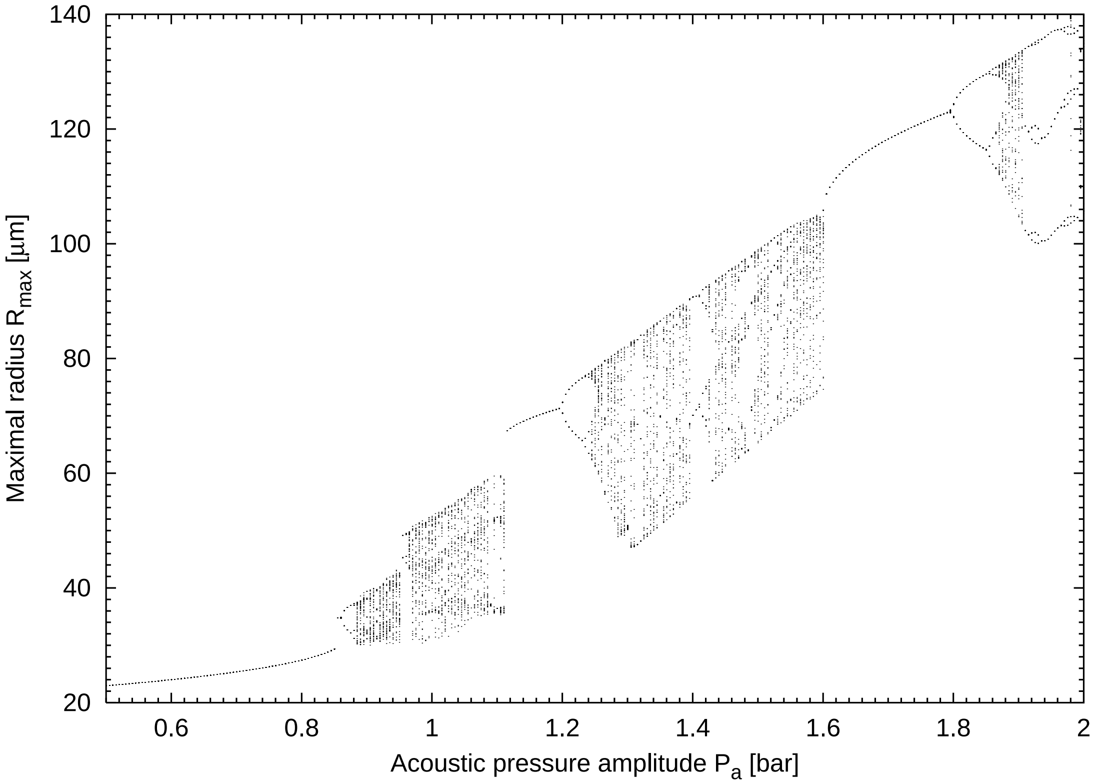

Figure 4: Bifurcation diagram of the maximum radius for $R_0 = 20\mu m$, $\gamma = 5/3$, and $\omega/2\pi = 27kHz$.

Since it is very time-consuming to map out numerically the whole parameter space, only the effect of changing the driving amplitude P_a is presented here. Such an analysis is usually carried out in a Poincare-section of the phase space, since it describes the dynamics just as well (by constructing a Poincare-map), and allows one to draw the parametric dependence in a plane. The choice of Poincare-section is arbitrary, the only necessary condition is that the trajectory should cross the plane of the section once every acoustic cycle. For driven systems one choice can be to get samples from a given part of each acoustic period. However a more general method, namely to set one of the phase space coordinates to zero, can also be applied. For this study the condition

$$P \equiv \max_{R}\{(R, V) \in \mathbf{R^2} : \mathit{V{=}0}\} \tag{8}$$

have been used, which gives the maximum radiuses from each acoustic period. Figure 4 shows the results for $R_0 = 20\mu m$, $\gamma = 5/3$, and $\omega/2\pi = 27kHz$. At each value of P_a the RP equation was solved for 100 cycles, and a Poincare-section was constructed by applying (8). Out of 100 cycles only the last 50 is shown on the figure, thus cutting out the uninteresting initial transients. For small enough forcing ($P_a \leq 0.85bar$) the dynamics is regular. Then a jump occurs, and the solution becomes chaotic after a period-doubling bifurcation sequence, showing the same qualitative features as reported in [4]. Inside the chaotic region one can observe windows of regular dynamics, just like in the case of the well-known logistic map. Figure 5 shows the return maps at different driving levels covering dynamics with 2-period, 4-period, chaos, and inside chaotic region a 3-period regime.

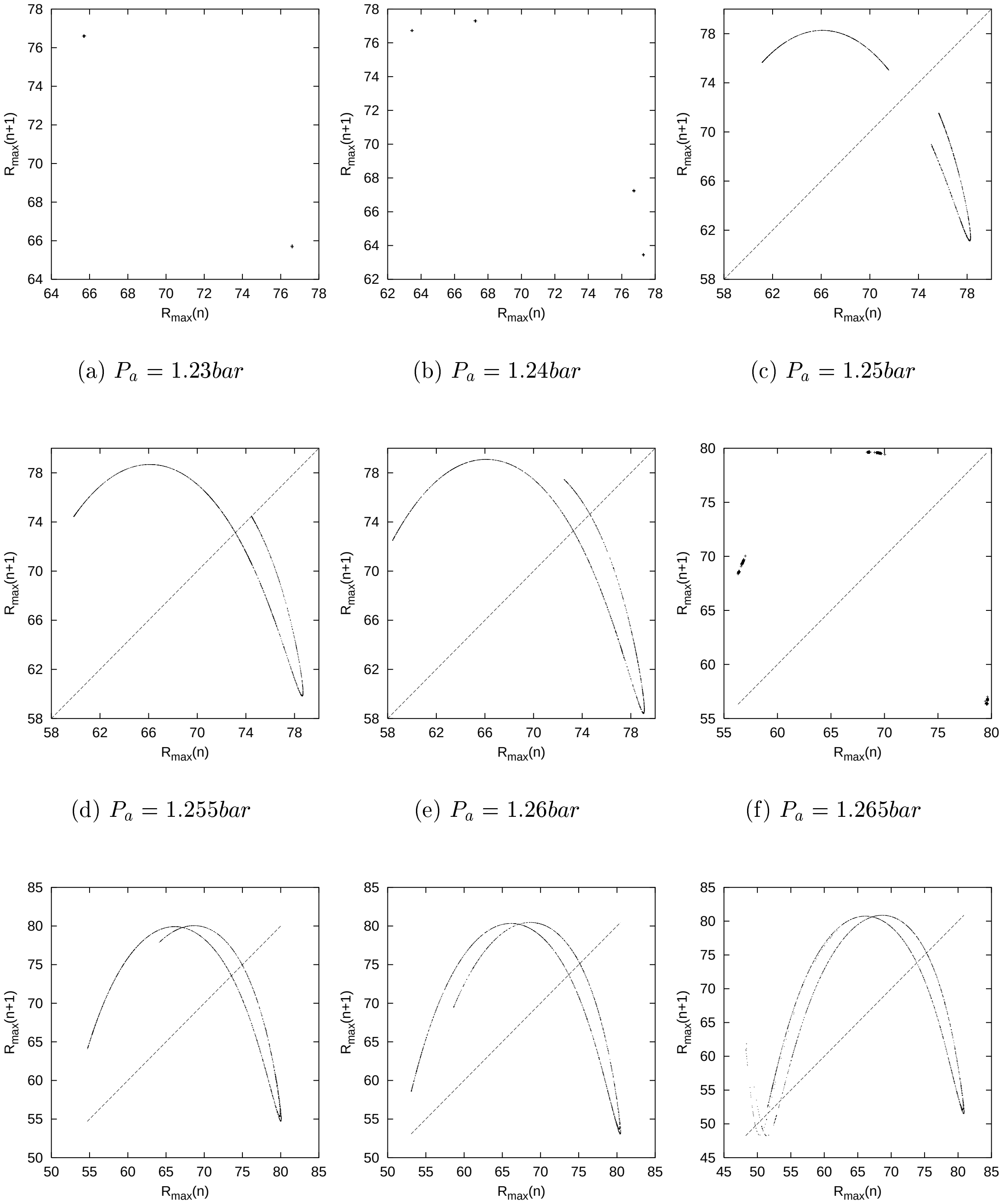

(a) $P_a = 1.23bar$ (b) $P_a = 1.24bar$ (c) $P_a = 1.25bar$

(d) $P_a = 1.255bar$ (e) $P_a = 1.26bar$ (f) $P_a = 1.265bar$

(g) $P_a = 1.27bar$ (h) $P_a = 1.275bar$ (i) $P_a = 1.28bar$

Figure 5: Return maps of maximal radii at different values of P_a. The other parameters are $R_0 = 20\mu m$, $\gamma = 5/3$, and $\omega/2\pi = 27kHz$.

Note the non-uniqueness and the increased complexity of the return maps with increased driving amplitude. Qualitatively the same kind of maps can be observed if the transition from regular dynamics to chaos is examined at driving levels around $0.88bar$ and $0.96bar$. In Fig. 6 another observable ξ is shown as a function of the driving level.

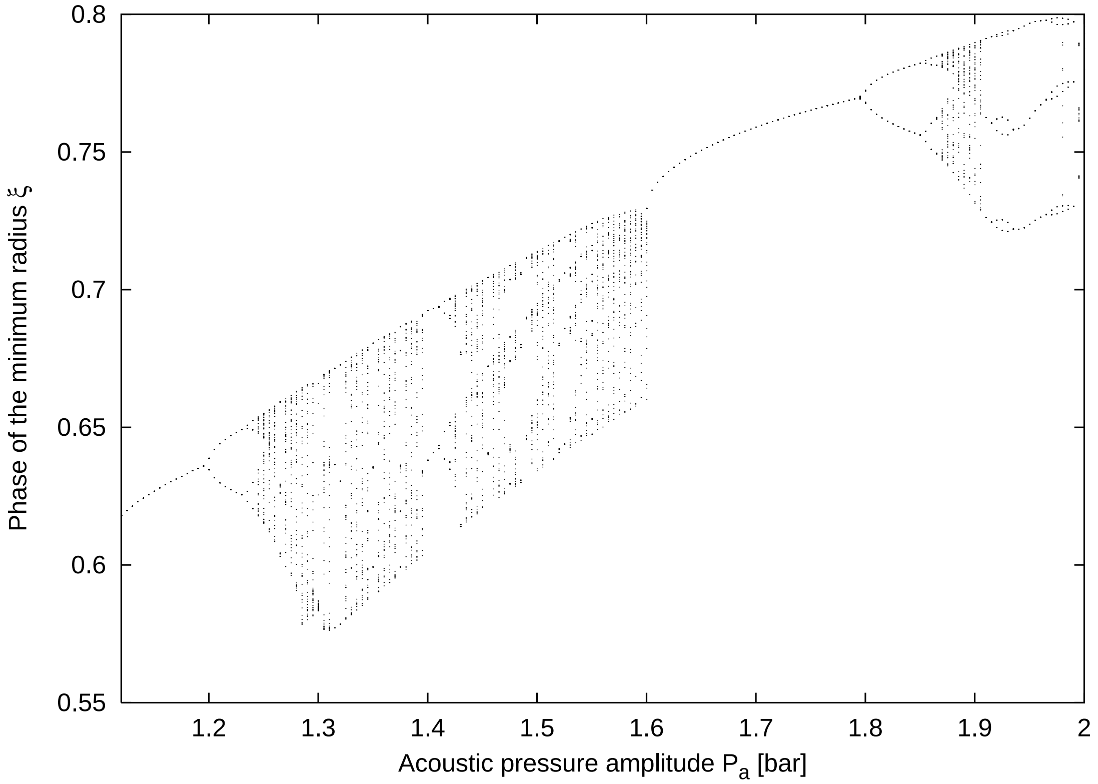

Figure 6: Bifurcation diagram of ξ for $R_0 = 20\mu m$, $\gamma = 5/3$, and $\omega/2\pi = 27kHz$.

It gives the phase of the minimal radius in the acoustic period, and defined as $\xi = t/T$, where t is the elapsed time from the beginning of the cycle until the radius reached its minimum, and T is the acoustic period. Trough this observable direct comparison can be made between simulation and measured data. Holt *et al* in [5] recorded the phases of subsequent flashes, which is the same quantity as ξ, since the light emission occurs at the minimal radius of the bubble. The extraction of minimal radiuses from each period also defines a Poincare section, but with a different condition

$$P \equiv \min_R\{(R, V) \in \mathbf{R^2} : \, V{=}0\} \tag{9}$$

Comparing Fig. 2 of [5] with Fig. 6 yields a reasonable agreement. Assuming that the pressure amplitude was around $P_a = 1.25bar$ in the measurement (not known exactly) they both give the result that ξ is distributed in an interval with length ≈ 0.05.

Although the Poincare sections described above are good for drawing bifurcation diagrams, or allow comparison with experiments, but for the purpose of finding periodic orbits and their stability the stroboscopic sampling method (sampling with the acoustic period) can be more fruitful for a harmonically driven system. This method produces return maps for both phase space coordinates (R,V). Figures 7 and 8 show the return maps for R and V respectively at different driving levels. The maps again get very complicated with increasing P_a, but at least there are parameter values where the return map of V reminds a horseshoe, implying that binary symbolic dynamics (possibly a pruned one) can be used to describe the system.

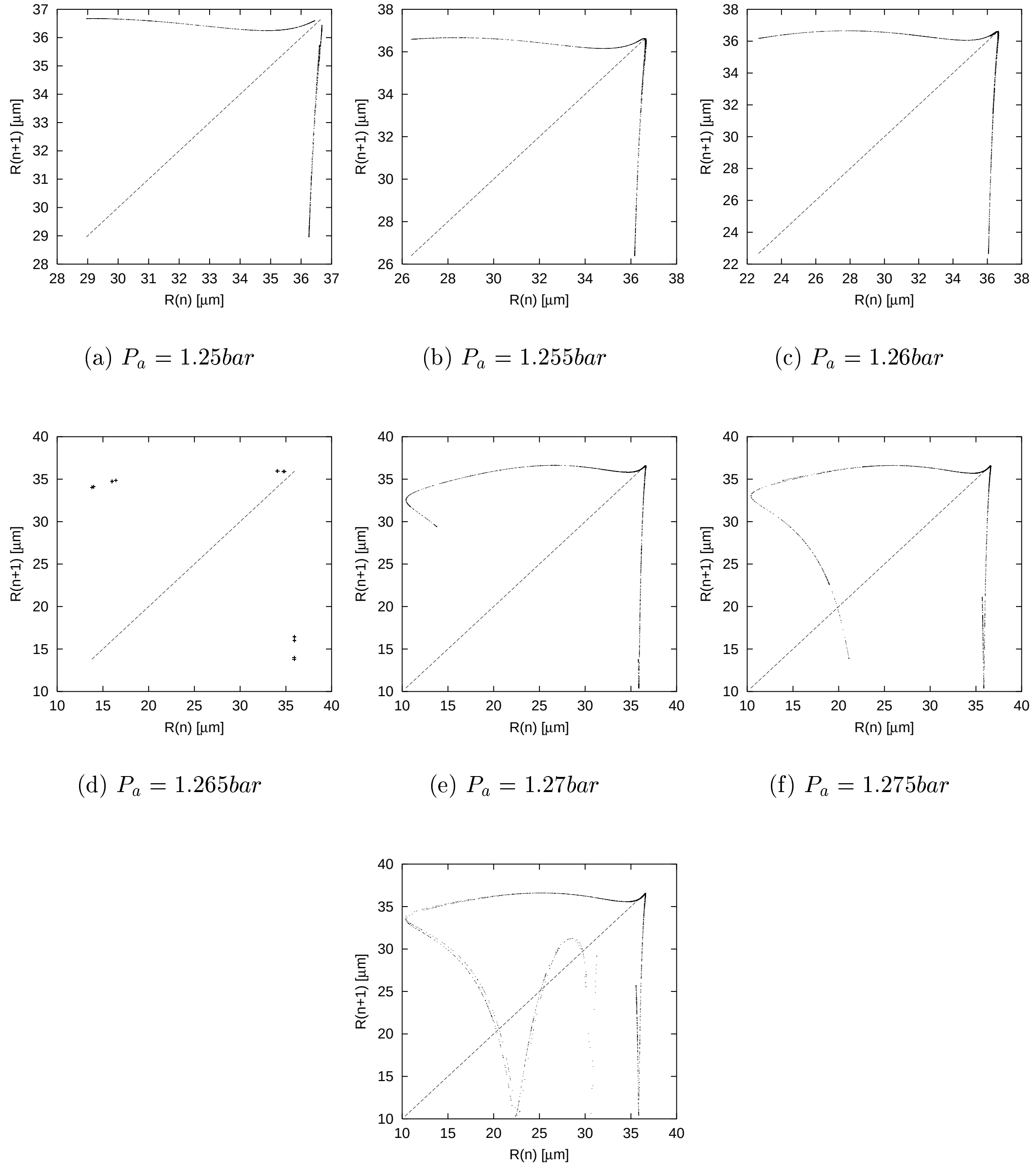

(a) $P_a = 1.25bar$

(b) $P_a = 1.255bar$

(c) $P_a = 1.26bar$

(d) $P_a = 1.265bar$

(e) $P_a = 1.27bar$

(f) $P_a = 1.275bar$

(g) $P_a = 1.28bar$

Figure 7: Return maps of bubble radius R, stroboscopically sampled at the end of each period. The other parameters are $R_0 = 20\mu m$, $\gamma = 5/3$, and $\omega/2\pi = 27kHz$.

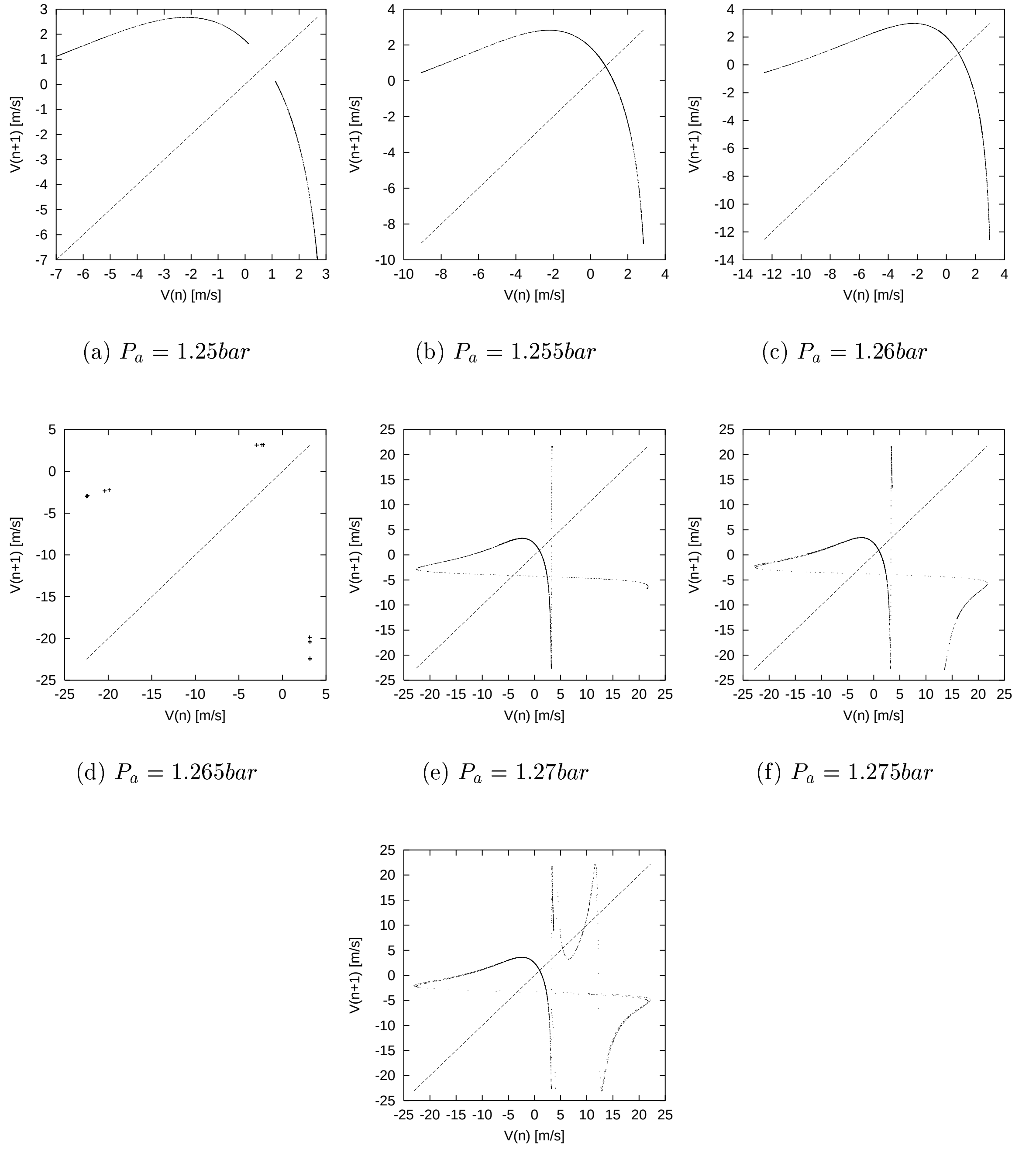

(a) $P_a = 1.25bar$ (b) $P_a = 1.255bar$ (c) $P_a = 1.26bar$

(d) $P_a = 1.265bar$ (e) $P_a = 1.27bar$ (f) $P_a = 1.275bar$

(g) $P_a = 1.28bar$

Figure 8: Return maps of the interface velocity V, stroboscopically sampled at the end of each period. The other parameters are $R_0 = 20\mu m$, $\gamma = 5/3$, and $\omega/2\pi = 27kHz$.

4 Detailed study of the system at chosen parameter values

This section gives the shortest periodic orbits up to length 5 and their stabilities, which together with the already known cycle periods (an integer times the acoustic period) can be plugged into cycle-expansions of trace formulas to compute averages of physical quantities [7]. All the simulations in this chapter used the parameters $P_a = 1.26bar$, $R_0 = 20\mu m$, $\gamma = 5/3$, and $\omega/2\pi = 27kHz$. The stability of a periodic orbit is given by the eigenvalues of the corresponding [d×d] dimensional Jacobian matrix, which is defined as

$$J^t_{i,j} = \frac{\partial f^t_i(\underline{x_0})}{\partial x_j} \qquad i,j \in \{1,..d\}, \tag{10}$$

where $f^t_i(\underline{x_0})$ is the i-th component of the solution with initial values $\underline{x_0}$, to the differential equations describing the dynamical system $\dot{\underline{x}} = \underline{v}(\underline{x},t)$ at the time instant t. In our case $d = 2$ and $\dot{\underline{x}} = \underline{v}(\underline{x},t)$ is represented by equations (3). The elements of the Jacobian can be computed by solving

$$\frac{d}{dt}J^t_{i,j} = \sum_{k=1}^{2} A_{i,k}(\underline{x},t)J^t_{k,j}, \qquad A_{i,k} = \frac{\partial v_i}{\partial x_k}, \tag{11}$$

along the orbit, with initial conditions $J^0_{i,i} = 1$ and $J^0_{i,j} = 0$, where $i \neq j$. The matrix $\underline{A}$ is called the derivative matrix, which is for the system in hand reads

$$\underline{A} = \begin{pmatrix} 0 & 1 \\ a_{21} & a_{22} \end{pmatrix} \tag{12}$$

with

$$\begin{aligned} a_{21} = & - \frac{1}{\rho_w R^2}(P_g - P_f - P_0 - P_\eta - P_\sigma + P_s) \\ & + \frac{1}{\rho_w R}\left(\frac{4\eta V}{R^2} + \frac{2\sigma}{R^2} - \frac{3\gamma R^2 P_g}{R^3 - a^3} + \frac{P_a}{c}\omega\cos(\omega t)\right) \\ & - \frac{9\gamma V P_g}{\rho_w c_w R}\left(\frac{R^2(R^3 - a^3) - R^5(1+\gamma)}{(R^3 - a^3)^2}\right) + \frac{3}{2}\frac{V^2}{R^2}, \end{aligned} \tag{13}$$

$$a_{22} = - \left(\frac{4\eta}{\rho_w R^2} + \frac{3\gamma R^2 P_g}{\rho_w c_w (R^3 - a^3)} + \frac{3V}{R}\right). \tag{14}$$

The expressions of the pressure terms P_g, P_f, P_η, P_σ and P_s, as a function of the phase space coordinates and time are already given in equations (2) and (4). An efficient way to find periodic orbits is to use the Newton-method sketched bellow. One starts with an initial guess $\underline{x}$ for the location of a fixed point in the Poincare-section, which is in our case $\underline{x} = (R, V)$ at time zero. Then one has to evolve the initial point, together with the Jacobian, and find their values $f(\underline{x})$ and J after an acoustic period. Inserting these into

$$\underline{x}' = \underline{x} - (1 - J)^{-1}(\underline{x} - f(\underline{x})), \tag{15}$$

yields the improved guess $\underline{x}'$. Iterating the routine the guesses converge faster then exponentially to the right values. In practice this means that for instance if one wishes to know the coordinates of a fixed point accurate to 10 digits, then it requires around 5-7 iterations, even if the initial guesses are quite rough. A problem can arise if the Jacobian has an eigenvalue 1 for some reason, because in that case the matrix $(1 - J)$ is not invertible. There are technics to overcome such difficulties (see chapter 9. of [7]), but fortunately in our case we do not have to deal with this problem.

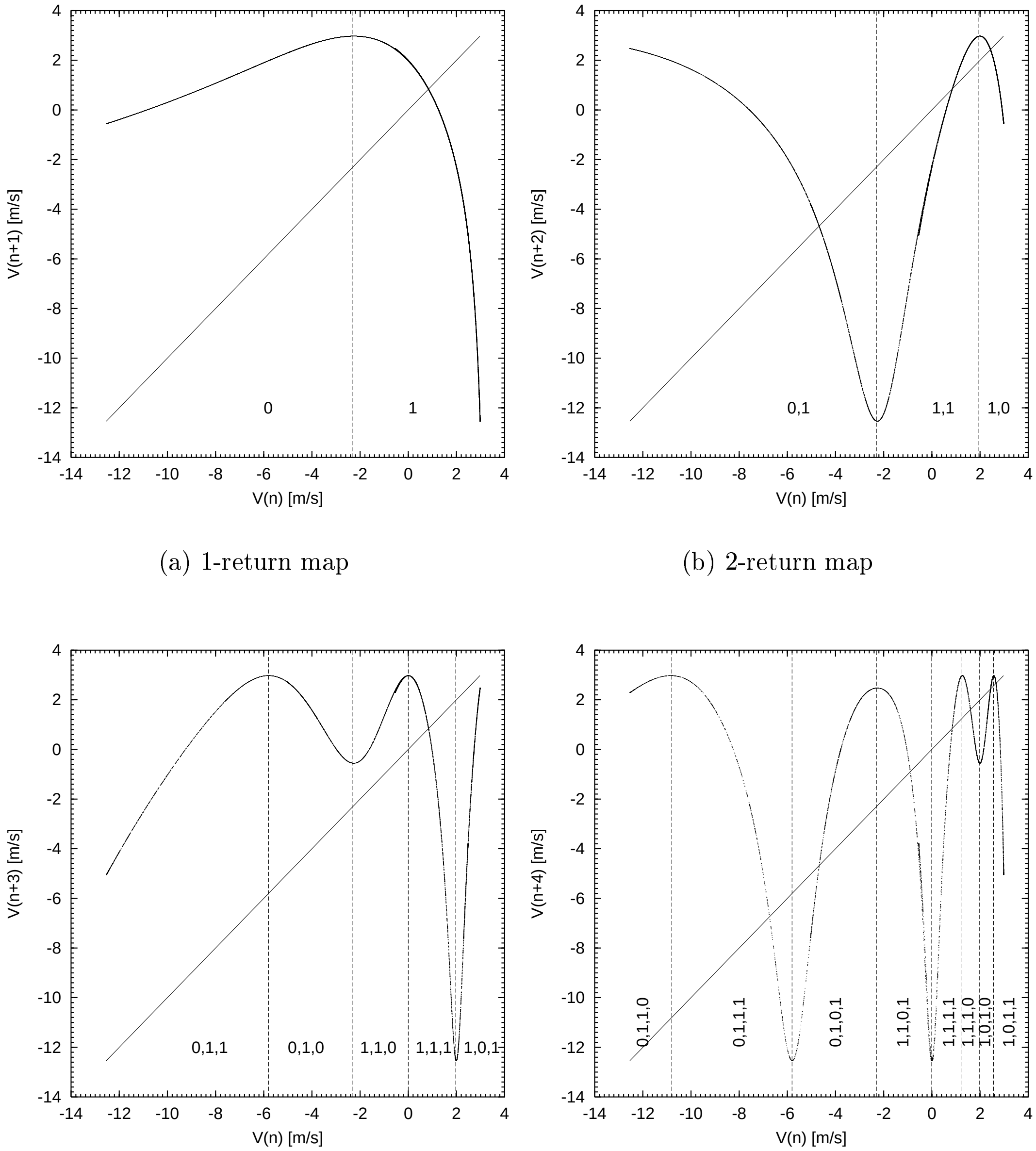

(a) 1-return map

(b) 2-return map

(c) 3-return map

(d) 4-return map

Figure 9: N-return maps of V. The vertical lines separate spatial regions with different itineraries. For instance if a trajectory is started from a region marked 0,1,0 it means that initially it was on the left of the 1-return map, in the next step it will be on the right side, and finally it will end up on the left.

Good starting values can be obtained from n-return maps of the phase space coordinate V, because a prime orbit of length n will show up as n identical fix points in such maps (see Fig. 9). The vertical line on the first return map identifies a value of V^* where the slope of the graph is 0, this special point is called the critical point.

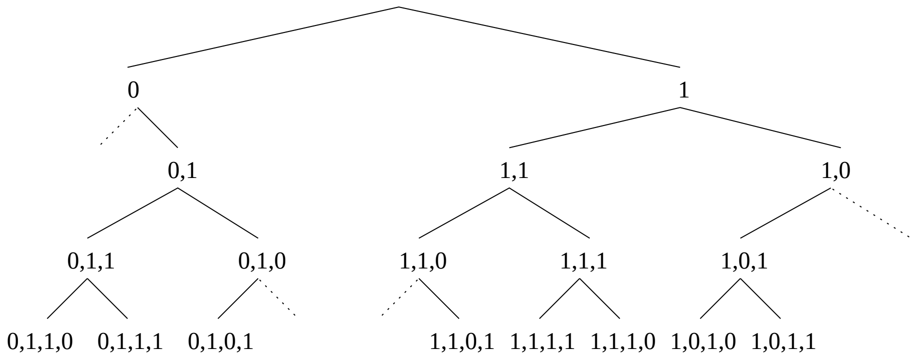

Figure 10: Admissible itineraries up to symbol-length 4. The dotted lines indicate pruning.

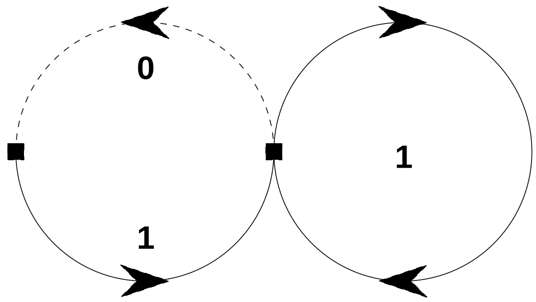

Figure 11: Markov-graph corresponding to the _00_ pruned binary tree. All symbol sequences of Fig. 10 can be generated as continuous walks on the graph along the arrows. The broken line corresponds to symbol 0, and the continuous line to 1. Roughly speaking the essence of the graph is that a symbol 0 always followed by 1, while 1 can be followed either by 1 or 0.

Introducing the following rules, the system can be described by a binary symbolic dynamics.

$$V(n) = \begin{cases} 0 & \text{if } V(n) < V^* \text{ (to the left from the crytical point)}, \\ 1 & \text{if } V(n) > V^* \text{ (to the right from the crytical point)}. \end{cases} \tag{16}$$

Using this definition the tree of admissible itineraries is constructed up to 4 letters (Fig. 10). The structure of the tree seems to obey the simple pruning rule that a letter 0 can not be followed by another 0. The corresponding Markov-graph is sketched in Fig. 11. Continuous walks on this graph generate all admissible itineraries. It is conjectured that all horseshoes will obey this pruning law if the V(n+1), which corresponds to the minimum V(n), is bigger than the critical value V^*, in other words if

$$V(n+1) > V^*, \text{ where } V(n+1) \text{ is such, that the corresponding V(n) is minimum.} \tag{17}$$

holds.[†] It must be noted that if an itinerary is admissible it does not in general mean that there is a prime periodic orbit corresponding to that symbol sequence. For instance ac-

[†]I do not know how to prove this with rigorous mathematics, but possibly it was already proven by somebody. If so, please let me know the reference, meanwhile Rytis is greatly encouraged to show me a counter-example.

cording to Fig. 9 there is not any prime 3-cycle, however there are 3 admissible itineraries with symbol length 3, which are cyclic permutations of each other. Given the Markov-graph of a system one can evaluate the topological entropy h

$$h = \lim_{n\to\infty} \frac{1}{n} K_n, \tag{18}$$

which tells how the number of admissible itineraries K_n, grows asymptotically with the length of the the itineraries n. The graph in Fig. 11 yields $h = ln((1+\sqrt{5})/2)$, which is the logarithm of the golden-mean (the computation is given in chapter 8. of [7]).The following tables list the prime cycles up to length 5, their stability eigenvalues, periods, Liapunov exponents, and the coordinates of the fixed point, where the Newton iteration converged. A part of the orbits is shown in Fig. 13.

n	word	Λ_s	Λ_u	Period T $[\mu s]$
1	1	-0.0030058775	-1.7541976455	37.037037037
2	1,0	-1.66193e-05	-2.7652591525	74.0740740741
3	-	-	-	-
4	1,0,1,1	-2.4e-10	-7.1953696659	148.1481481481
5	1,0,1,1,1	2e-12	7.5841781572	185.1851851852
5	1,0,1,1,0	-2e-12	-6.2755375293	185.1851851852

Table 2: Stable and unstable eigenvalues of the Jacobian, and the period of the orbits

n	word	$\lambda = ln(\|\Lambda_u\|)/T$ [1/s]	R $[\mu m]$	V [m/s]
1	1	15174.31239	36.5876651173	0.8312625423
2	1,0	13731.31382	36.3527602712	2.42507375674
3	-	-	-	-
4	1,0,1,1	13320.71791	36.2272815784	2.65570357403
5	1,0,1,1,1	10940.74698	36.1026785372	2.8891562482
5	1,0,1,1,0	9917.959374	36.0861125528	2.9268794801

Table 3: Liapunov exponents and the coordinates of fixed points.

The information contained in the stability and period of prime periodic orbits can be used to calculate global properties, such as Liapunov exponent, or averages of physical quantities of interest for the particular system. For instance in our case this quantity can be the concentration of the gas in the liquid C_i, at which the bubble is in diffusive equilibrium with the surroundings. For stable periodic oscillations this is given by

$$C_i/C_0 = \frac{\int_0^T R(t)^4 P_g(R(t))dt}{P_0 \int_0^T R(t)^4 dt}, \tag{19}$$

where C_0 is the constant equilibrium air-concentration at an ambient pressure of 1 bar, and the integration is done over one acoustic period (see i. g. [10]). If the oscillations are chaotic one have to do the integrals above over a very long time, until the trajectory covers the whole attractor (Fig. 3). According to [7] the average over the covered part of the phase space can be rewritten as an average over the unstable periodic orbits.

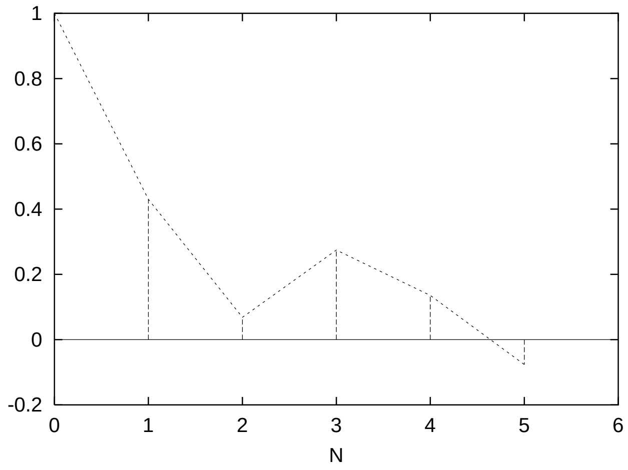

Figure 12: The convergence of escape rate to zero, with increasing topological length of truncation.

Before proceeding any further, it is worth to note, that the system satisfies the hyperbolicity assumption (at least in the case of the few studied orbits), which is a requisite to apply the forthcoming methods (see chapter 6. of [7]). Skipping a lot of details and considerations, (which can be found in [7], here we just state that for bound system with zero escape rate the phase space average of a time-integrated quantity A can be expressed through an infinite sum over the properties of the prime periodic orbits

$$\langle A \rangle = \sum_{\{p_1,p_2..p_k\}}^{\prime} (-1)^{k+1} \frac{A_{p_1} + A_{p_2} ... + A_{p_k}}{|\Lambda_{p_1} \Lambda_{p_2} ... \Lambda_{p_k}|} \tag{20}$$

where the sum is taken over all distinct nonrepeating combinations of prime cycles with topological length k ($k = 1..\infty$), Λ_{p_k} is the expanding eigenvalue of the Jacobian evaluated along the orbit, and A_{p_k} denotes that the physical quantity is integrated in time over the orbit period T_{p_k}. In practice one always uses a truncated version of the above formula, but that still gives good approximations, since the contribution of cycles diminishes with their topological length. For convenience the truncated (at topological length 5) version of equation (20) applied for the system at hand is shown bellow

$$\langle A \rangle = \frac{A_{p_1}}{|\Lambda_{p_1}|} + \frac{A_{p_{10}}}{|\Lambda_{p_{10}}|} + \frac{A_{p_{1011}}}{|\Lambda_{p_{1011}}|} + \frac{A_{p_{10111}}}{|\Lambda_{p_{10111}}|} + \frac{A_{p_{10110}}}{|\Lambda_{p_{10110}}|} - \frac{A_{p_1} + A_{p_{10}}}{|\Lambda_{p_1} \Lambda_{p_{10}}|} - \frac{A_{p_1} + A_{p_{1011}}}{|\Lambda_{p_1} \Lambda_{p_{1011}}|}. \tag{21}$$

The validity of the approximation can be checked by flow conservation sum rules such as

$$0 = 1 - \sum_{\{p_1,p_2..p_k\}}^{\prime} (-1)^{k+1} \frac{1}{|\Lambda_{p_1} \Lambda_{p_2} ... \Lambda_{p_k}|} \tag{22}$$

which is exact if the sum involves infinite cycles. This formula gives the escape rate of trajectories, which for bounded system equals zero. Figure 12 shows to what degree equation (22) is satisfied as a function of the truncation. The non-monotonous, and relatively slow convergence can be attributed to the effect of pruning, since in this case there is only partial shadowing. For instance there is not any 101-term present which would almost cancel the affix of the 1·10-term, thus there is a hump in Fig. 12 at N=3. Another message of this figure is that if one wishes to obtain more accurate results, than a calculation of a few more cycles is necessary.

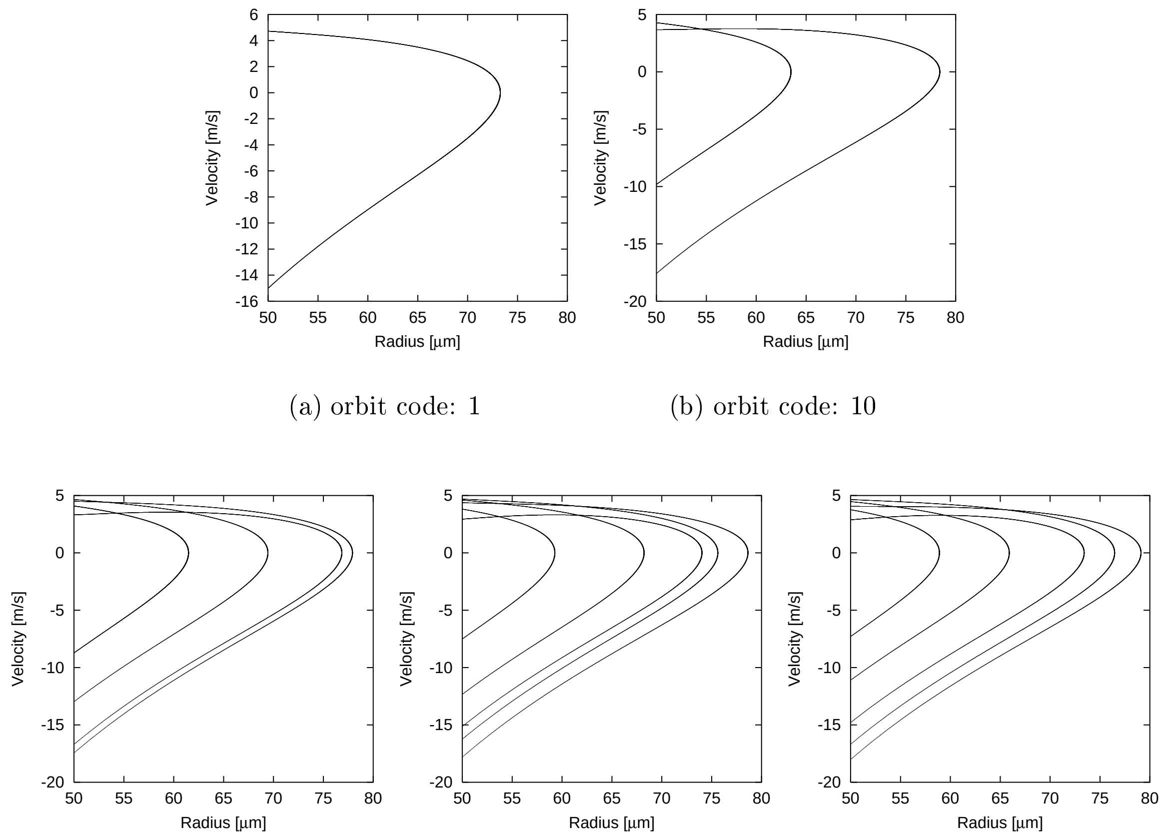

(a) orbit code: 1 (b) orbit code: 10

(c) orbit code: 1011 (d) orbit code: 10111 (e) orbit code: 10110

Figure 13: Prime periodic orbits up to topological length of 5 symbols. The pictures show a blowup of the phase space near the maximum radius.

5 Averages of physical quantities

This section gives the results of applying the method discussed in the previous section for the dimensionless equilibrium concentration C_i/C_0. Water at normal conditions contains an amount of dissolved air with concentration C_0. In experiments one usually sets C_i to be a fraction of the normal value to achieve equilibrium, otherwise the bubble would grow from cycle to cycle by rectified diffusion [10]. It is worth to mention that in the applications the acoustic period is much smaller than the timescale of diffusion. If this would not hold, one would have to use a modified RP equation which incorporates diffusion. For convenience equation (19) is rewritten in a form

$$C_i/C_0 = \frac{A_p}{B_p}, \qquad A_p = \int_0^{T_p} R(t)^4 P_g(R(t))dt, \qquad B_p = P_0 \int_0^{T_p} R(t)^4 dt. \tag{23}$$

The following table 4 contains the values of A_p and B_p obtained for the shortest cycles. Using the data of table 4, 3 and equation (21) the result for the equilibrium concentration is

$$C_i/C_0 = \langle A \rangle \, / \, \langle B \rangle = 0.01361. \tag{24}$$

n	word	A_p	B_p
1	1	3.65727e-19	2.76979e-17
2	1,0	7.3425e-19	5.44125e-17
3	-	-	-
4	1,0,1,1	1.46754e-18	1.08642e-16
5	1,0,1,1,1	1.83594e-18	1.34183e-16
5	1,0,1,1,0	1.83734e-18	1.33479e-16

Table 4: The values A_p and B_p integrated over the periods of the calculated prime orbits.

This means that in order to be in diffusive equilibrium with the surrounding liquid the water has to be de-gassed to 1.36% of its concentration at normal conditions. For stable oscillations it is customary (and satisfactory) to calculate the above integrals only for one acoustic cycle, and with initial values $R(t=0)=R_0$, $V(t=0)=0$. The question can arise how big error will one get by applying these rules for the chaotic case. The calculation for C_i/C_0 in this case gives 0.0301, which is a considerable difference. One can also check how good approximation can be obtained by considering only the first prime periodic orbit. In this case one gets $C_i/C_0 = 0.0132$, a value very close to the one obtained with 5 prime cycles. This suggests that in the parameter space where the oscillations are chaotic one can not use the usual methods (averaging for one acoustic cycle, with initial conditions $R(t=0)=R_0$, $V(t=0)=0$), but forced to apply alternative technics like the one presented in this study. We have showed that making the averages on the first unstable prime cycle already produces reasonably good results.

6 Consequences for single bubble sonoluminescence

As mentioned in the introduction, the period doubling and chaotic behaviour of the RP equation (though of a bit different form) was already investigated in 1984 [4] for big bubbles ($R_0 = 100\mu m$ and $230\mu m$), at a driving frequency of $23.56kHz$, and driving amplitudes up to $P_a = 10bar$. The part of the parameter space where single bubble sonoluminescence was observed in experiments so far, can be roughly given as $P_a = 0.9-2bar$, $\omega/2\Pi = 10-40kHz$, and $R_o = 1-7\mu m$. In particular the measurement of Holt *et al*, which reported period-doubling and chaos in the time series of subsequent light flashes, was made at $27kHz$, and $R_0 \sim 5\mu m$, $P_a \sim 1.3bar$ [5]. Although it was proposed that the observed chaos could originate directly from RP dynamics, no systematic study proved this conjecture. Peter Snoer Jensen addressed this question in his thesis [6], and using ideal gas law with adiabatic equation of state successively reproduced the desired dynamics in the parameter range of SBSL. Nevertheless his conclusion on this matter can not be taken as a proof, because in modelling SBSL the use of the van der Waals equation of state is essential [2], moreover the validity of adiabatic process is also questionable. According to [3] in most of the acoustic cycle, except for the nanoseconds of wild collapse, the gas inside the bubble will be isothermic with the surrounding liquid, implying that $\gamma = 1$ is a more realistic choice.

To provide a detailed study the parameter region of SBSL was scanned for the stability of solutions to the RP equation, using the van der Waals EOS (2), and different polytropic exponents.

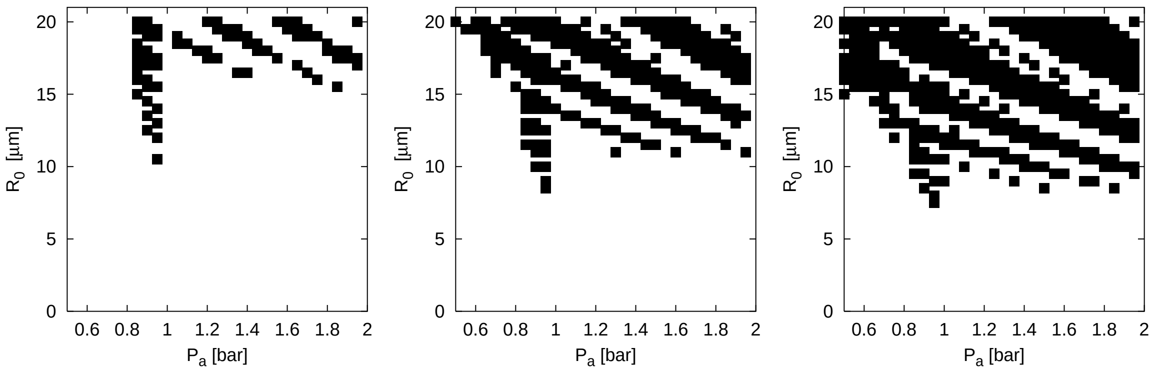

(a) Frequency = 17 kHz. (b) Frequency = 27 kHz. (c) Frequency = 37 kHz.

Figure 14: Stability of the RP-equation assuming isothermic EOS ($\gamma = 1$) in the $(P_a, R_0, \omega/2\pi)$ parameter space. In the shaded regions condition (25) is satisfied, implying that transients of R_{max} after 10 cycles still stayed above 0.1%. Note the resonance-like structure of stability (stripes) inside the dark areas.

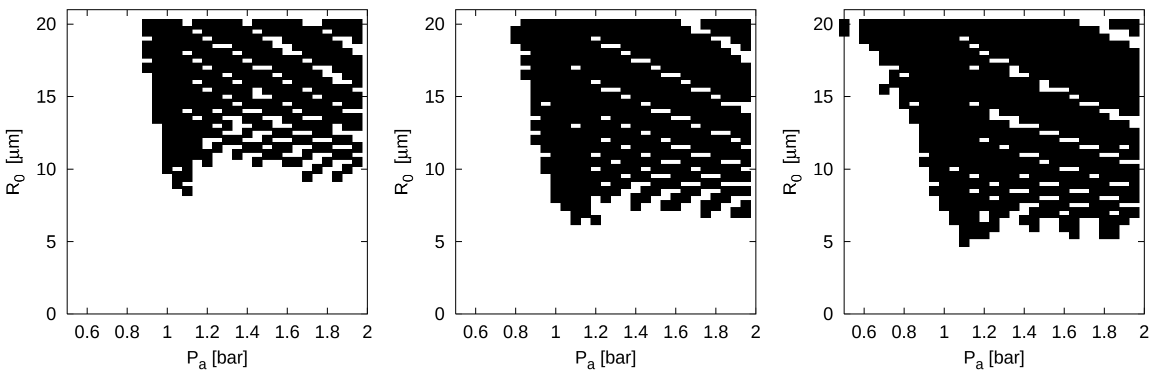

(a) Frequency = 17 kHz. (b) Frequency = 27 kHz. (c) Frequency = 37 kHz.

Figure 15: Stability of the RP-equation assuming adiabatic EOS ($\gamma = 5/3$). All the other parameters were kept the same as in Fig 14.

To make the simulations more realistic the value of $0.05N/m$ were used for the surface tension (see the footnote on Page 2.). For all the other material constants their tabular values (listed in Table 1) were chosen. At each point in the parameter space $(P_a, R_0, \omega/2\pi)$ the RP equation was solved for 10 acoustic periods, and the values of maximal radiuses R_{max} from each cycle were extracted. The condition

$$S \equiv \|\frac{R_{max}^{(9)} - R_{max}^{(10)}}{R_{max}^{(9)}}\| \geq \xi_{tr} \tag{25}$$

was used to identify parameter space points where the transients after 10 cycles still stayed above a chosen threshold value ξ_{tr}. Figure 14 shows the results for $\xi_{tr} = 0.001$ and $\gamma = 1$.

The same simulations for an adiabatic EOS with $\gamma = 5/3$ are shown in Fig. 15. Several trends are apparent from these figures. First of all the use of $\gamma = 1$ enhances the stability, and the lowering of the excitation frequency has the same effect. Still it can be observed that there are points in the parameter space of SBSL where the transients did not die out in 10 cycles in the adiabatic case. To check the boundary of the relevant parameter space more detailed simulations need to be performed allowing for bigger transient time. An investigation of the role of the ambient pressure P_0, and of water temperature (which changes the material constants in the equation) still could result in chaotic RP dynamics inside the parameter range of SBSL and thus explain the observation of the measurements.

7 Conclusion

The RP dynamics of a driven gas bubble has been investigated in the stable and chaotic regime. All the findings of a previous study [4] obtained for "big bubbles" ($R_0 \geq 100\mu s$) concerning period doubling, and chaos were observed in a parameter range which is closer to the parameter space relevant for single bubble sonoluminescence. Periodic orbit theory has shown to be a powerful tool for calculating physical quantities in the chaotic regime, where the standard methods used in modelling SBSL would break down. By scanning the parameter range of SBSL with a more realistic model than used in [6], all the transients found to die out in less then 10 cycles. This implies that the solutions to the RP equation are stable in the whole parameter space of SBSL at least at normal conditions (room temperature, 1 bar static pressure), thus leaving the question of the origin of chaos observed in measurements [5], [6] open.

8 Acknowledgements

Anders Andersen is thanked for driving my attention on the M.Sc. thesis of Peter S. Jensen and loaning me his copy. Peter S. Jensen is thanked for writing it in the first place, Rytis Paskauskas is thanked for valuable discussions and hospitability (chicken), finally Csabai Istvan is also thanked for valuable discussions, and for providing access and full priority on the super-computer (Redshift) at the Eotvos University, while other term-project writers (Rytis) were slowing down Alf.

References

[1] Lord Rayleigh, Phil. Mag. 34, 94 (1917); M. Plesset, J. Appl. Mech. 16, 277 (1949); Ritva Löfstedt, Bradley P. Barber, and Seth J. Putterman, Phys. Fluids A 5, 2911 (1993).

[2] Bradley P. Barber *et al*, Phys. Rep. 281, 65 (1997).

[3] Andrea Prosperetti, J. Acoust. Soc. Am. 61, 17 (1977).

[4] Werner Lauterborn and Engelbert Suchla, Phys. Rev. Lett.53, 2304 (1984).

[5] R. Glynn Holt, D. Felipe Gaitan, and Antony A. Atchley, Phys. Rev. Lett. 72, 1376 (1994).

[6] Peter S. Jensen, M.Sc. thesis, Niels Bohr Institute/CATS,(1998).

[7] Predrag Cvitanovich *et al*, Classical and Quantum Chaos Webbook, http://www.nbi.dk/ChaosBook/.

[8] William H. Press *et al*, Numerical Recipes in C.

[9] Hao Bai-lin, Elementary Symbolic Dynamics and Chaos in Dissipative Systems, World Scientific 1989.

[10] A. Prosperetti, Quart. Appl. Math. 34, 339 (1977); M.P. Brenner, D. Lohse, and T .F. Dupont, Phys Rev. Lett. 75, 954 (1995); S. Hilgenfeldt, D. Lohse, and M.P. B renner, Phys. Fluids 8, 2808 (1996); C.C. Wu, P.H. Roberts, Phys. Lett. A, 250, 131 (1998)